Geophysical Research Letters

RESEARCH LETTER
10.1029/2020GL089311

Interannual Variability of Lower Equatorial Intermediate Current Response to ENSO in the Western Pacific

Qiang Ma[1,2,3,4], **Jianing Wang**[1,2,3,4], **Fan Wang**[1,2,3,4], **Dongxiao Zhang**[5,6], **Zhixiang Zhang**[1,2,3,4], **and Yilong Lyu**[1,2,3]

[1]Key Laboratory of Ocean Circulation and Waves, Institute of Oceanology, Chinese Academy of Sciences, Qingdao, China, [2]Function Laboratory for Ocean Dynamics and Climate, Pilot National Laboratory for Marine Science and Technology Qingdao, Qingdao, China, [3]Center for Ocean Mega-Science, Chinese Academy of Sciences, Qingdao, China, [4]University of Chinese Academy of Sciences, Beijing, China, [5]Joint Institute for the Study of the Atmosphere and Ocean, University of Washington, Seattle, WA, USA, [6]Pacific Marine and Environmental Laboratory, NOAA, Seattle, WA, USA

Abstract The ocean currents of the tropical Pacific Ocean vary with El Niño-Southern Oscillation (ENSO) cycles. A mooring time series obtained during 2014–2018 in the western Pacific reveal that interannual variability extends to Lower Equatorial Intermediate Current (LEIC). The LEIC velocity anomalies are significantly correlated with the Niño-3.4 index at an 11-month lag. Monthly velocity data from the global ocean physical reanalysis product and from a linear continuously stratified ocean model during 1993–2018 capture the 2015–2016 signal and are used to identify the underlying mechanism. During El Niño (La Niña) events, the direct wind forcing in the central tropical Pacific and the reflection of Kelvin waves in the eastern Pacific during the first autumn-winter period contribute comparably to an eastward (westward) current anomaly in the western Pacific during the second autumn-winter period. This process is achieved mainly through the generation of the second baroclinic mode and off-equatorial westward-propagating downwelling (upwelling) Rossby waves.

Plain Language Summary The El Niño-Southern Oscillation (ENSO) is interconnected with the interannual variability of upper ocean circulation. Through analyzing a 4-year mooring observation and a 26-year reanalysis product at 0°, 142°E, we find that the interannual variability of the Lower Equatorial Intermediate Current (LEIC) lying between 600 and 820 m is also influenced by ENSO. The LEIC flows westward during boreal autumn-winter and reverses to an eastward-flowing current during spring-summer. However, in the following year of El Niño events, the westward-flowing LEIC disappears during autumn-winter. With the aid of a linear continuously stratified ocean model, we demonstrate that the absence of the LEIC during this period is mainly related to pressure anomaly fields at intermediate depths caused by the off-equatorial westward-propagating first meridional and second baroclinic modes downwelling Rossby waves. These Rossby waves are generated by the anticyclonic wind stress curl associated with the easterly wind anomaly in the eastern Pacific and by the eastern boundary reflection of equatorial Kelvin waves initially triggered by the westerly wind anomaly in the central Pacific during the mature stage of El Niño events. The above two originations make comparable contributions to the interannual variability.

Key Points:
- Lower equatorial intermediate zonal current anomaly is significantly correlated with Niño-3.4 index at an 11-month lag
- Equatorial intermediate interannual variability is related to second baroclinic mode Rossby waves mainly generated by ENSO mature stage wind
- Rossby waves from direct wind forcing and reflection of Kelvin waves contribute comparably to intermediate interannual variability

Supporting Information:
- Supporting Information S1

Correspondence to:
J. Wang and F. Wang,
wjn@qdio.ac.cn;
fwang@qdio.ac.cn

Citation:
Ma, Q., Wang, J., Wang, F., Zhang, D., Zhang, Z., & Lyu, Y. (2020). Interannual variability of Lower Equatorial Intermediate Current response to ENSO in the Western Pacific. *Geophysical Research Letters*, *47*, e2020GL089311. https://doi.org/10.1029/2020GL089311

Received 12 JUN 2020
Accepted 30 JUL 2020
Accepted article online 6 AUG 2020

1. Introduction

The Equatorial Intermediate Current (EIC) system contributes to global circulation, climate variability, and distributions of heat, watermass, and biogeochemical quantities (e.g., Ascani et al., 2015; Brandt et al., 2011; Czeschel et al., 2011; Hu et al., 2015; Margolskee et al., 2019; Stramma et al., 2010). As a major component of the EIC system in the Pacific Ocean, the westward-flowing Lower Equatorial Intermediate Current (LEIC) is found beneath the Equatorial Undercurrent (EUC) and EIC between 2°N and 2°S, ranging from 600 to 1,200 m with a core at ~800 m. The LEIC weakens and shoals toward the east (Cravatte et al., 2017; Marin et al., 2010).

A recent review by Ménesguen et al. (2019) summarizes observations and formation mechanisms of intermediate currents and stresses the important role of deep equatorial intraseasonal variability in their formation. Furthermore, the EIC and LEIC seasonal variations and their underlying mechanisms have been well studied. The mean westward-flowing EIC and LEIC can seasonally reverse to eastward-flowing currents,

which have been observed in various meridional sections (Cravatte et al., 2017; Firing, 1987; Firing et al., 1998; Gouriou et al., 2006). Such a seasonal cycle is generated by the vertical propagation of the first meridional mode ($l = 1$) Rossby wave, which is directly forced by the westward-propagating annual equatorial zonal wind fields (Kessler & McCreary, 1993; Marin et al., 2010).

Due to the sparse and fragmented observations, the interannual variability of LEIC is rarely studied. Under the dominant influence from the El Niño-Southern Oscillation (ENSO), the upper equatorial currents in the Pacific, including the EUC, the South Equatorial Current (SEC), and the North Equatorial Countercurrent, have exhibited significant interannual variability (e.g., Izumo, 2005; Johnson et al., 2000; Shinoda et al., 2011; Zhao et al., 2013). Using 16-month time series current measurements at 159°W spanning the 1982–1983 El Niño episode, Firing (1987) revealed that the zonal currents at EIC and LEIC depths were westward in May 1982 but eastward in May 1983. A similar interannual signal was also detected at 138°E with a 4-year continuous record from moored current meters during 1998–2002 (Kawabe et al., 2008). The underlying dynamics of the interannual variability, however, were not discussed in these studies. Based on Argo gridded temperature-salinity data and drifting velocity data, Johnson and Birnbaum (2016) revealed a strengthening of the westward-flowing EIC in the western Pacific 3 months after the peak of an El Niño. However, these Argo data are still insufficient to robustly determine the mechanisms that drive the interannual variability of the Pacific EICs (Zanowski et al., 2019). Nevertheless, investigating the mechanisms of intermediate currents at the interannual timescale is very important for climate and oceanographic research. This will help us to understand how and why the intermediate currents respond to climate variability and change.

From September 2014 to December 2018, a subsurface mooring was deployed at 0°, 142°E to monitor the variability of LEIC. This mooring is a part of the Scientific Observing Network of the Chinese Academy of Sciences in the western Pacific (Lyu et al., 2018; Ma et al., 2019; Song et al., 2018; Wang et al., 2016: Wang, Wang, et al., 2016). The temporal coverage of the mooring data allows the investigation of the interannual variability of LEIC in response to the strong 2015–2016 El Niño event. Our approach is to combine data analyses on mooring observation, reanalysis product, and numerical experiments with a linear continuously stratified (LCS) ocean model.

2. Data

2.1. Mooring Data

The subsurface mooring has one upward- and one downward-looking TRDI (Teledyne RD Instruments) 75 kHz Acoustic Doppler Current Profilers (ADCPs) mounted on the main float at ~500 m. The ADCPs returned the velocity profiles over the depth range of 50–950 m with a vertical bin size of 8 m and a frequency of 35 pings per hour. The data were first interpolated vertically to 1-m intervals and then averaged to derive the monthly mean for analysis.

2.2. LCS Model

To elucidate the wind-driven equatorial wave dynamics, the LCS ocean model is used. This model is configured to the Pacific Ocean between 20°S to 20°N and 100°E to 70°W with horizontal resolutions of 0.25° × 0.25°. The background potential density is obtained from World Ocean Atlas 2013 temperature and salinity data averaged over 5°S to 5°N and 130°E to 80°W. The resultant profile is then interpolated from 0 m to 4,000 m with a 10 m vertical resolution. Vertical modes are computed based on background density, and the characteristic wave speeds (c_n) for the first four baroclinic modes are 266, 159, 100, and 72 cm s^{-1}, respectively. These values are consistent with those of a similar computation in Yu and McPhaden (1999). For model equations and parameterizations, readers can refer to Chatterjee et al. (2013); Huang et al. (2018); and Shankar et al. (1996). In this study, the total solution is the sum of the first 10 baroclinic modes. The model is first spun up for 10 years forced by the monthly mean climatology of cross-calibrated multiplatform (CCMP) satellite winds during 1993–2018 (Atlas et al., 2008). The climatology run is then used as the restart state for all the other solutions. The main run, referred to as LCS-MR, intergrates forward in time for the period of 1993–2018 using monthly CCMP winds.

2.3. Reanalysis Product

To investigate the interannual variability of LEIC over a longer period than the observation, we use monthly velocity data during 1993–2018 from the global ocean physical reanalysis product GLORYS12V1 (hereinafter

GL12) created by Mercator Ocean. The product has a horizontal resolution of 1°/12° in longitude/latitude and 50 vertical levels. For more details on the reanalysis product, readers are referred to Lellouche et al. (2018).

3. Result

Figure 1a presents the time-depth variations of observed monthly zonal currents at 0°, 142°E. Four dominant zonal currents in the upper 950 m are revealed: the westward-flowing SEC in the upper 130 m with a core of mean velocity reaching 17 cm s^{-1} at ~90 m (Figure S1 in the supporting information), the eastward-flowing EUC between 130 and 340 m depths with a core of mean velocity reaching 40 cm s^{-1} at ~230 m, and the two westward-flowing currents EIC between 340 and 490 m and LEIC below 600 m with separate cores of mean velocities exceeding 10 cm s^{-1} at ~420 m and 5 cm s^{-1} at ~700 m, respectively.

For the EIC and LEIC, two striking features are revealed in the observation. First, a pronounced seasonal cycle was present with a strong westward-flowing phase during autumn-winter (boreal, same hereinafter) and a weak westward- or even eastward-flowing phase during spring-summer in 2014, 2015, 2017, and 2018. Second, unlike the above years, the strong westward-flowing phase atypically disappeared during autumn-winter in 2016 (Figure 1a), exhibiting significant interannual variability. This is particularly true for LEIC, which reversed to an eastward-flowing current during this period. The zonal current anomaly (U_a, seasonal cycle removed) averaged over 600–820 m (depth of 820 m is selected according to the depth of available ADCP data) has the largest correlation of 0.82 with the Niño-3.4 index at an 11-month lag (Figure 1j). The correlation coefficients here and subsequently are all significant at the 95% confidence level. This suggests that the atypically disappeared LEIC (i.e., strong eastward U_a) during autumn-winter in 2016 may be related to the 2015–2016 El Niño event (Figures 1e and 1f). Next, we will focus on the mechanisms underlying the LEIC interannual variability with the aid of GL12 and LCS.

The performance of GL12 and LCS in simulating the LEIC is first examined. During the mooring measurement period, the aforementioned two striking features in LEIC are successfully reproduced in GL12 and LCS-MR (Figures 1b and 1c). The correlation coefficients (r) between the observed and modeled U_a at the mooring site are significant ($r > 0.52$) at the LEIC depths (Figure S1). Additionally, the GL12 and LCS-MR monthly U_a averaged over 600–820 m at the mooring site agree reasonably well with the observation (Figure 1d). High correlation coefficients of 0.82, 0.82, and 0.79 are exhibited between observation and GL12, observation and LCS-MR, and GL12 and LCS-MR, respectively. Note that both GL12 and LCS-MR show a poor performance in the EIC interannual variability ($r < 0.3$; Figure S1). This is likely due to the overlapped depth ranges of EUC and EIC, which cannot be well reproduced by the models (Figures 1a–1c).

For a longer period during 1993–2018, the correlations of U_a in GL12 and LCS-MR with the Niño-3.4 index (Figure 1g) both show a peak value larger than 0.61 at an approximately 11-month lag (Figure 1j). This adds solid evidence that the LEIC interannual variability is closely associated with ENSO. Following the NOAA definition, an El Niño (La Niña) event is defined as a period when the 3-month running-mean of Niño-3.4 exceeds 0.5°C (falls below −0.5°C) for at least five consecutive months. During each 2-year El Niño event (i.e., 1994–1995, 1997–1998, 2002–2003, 2004–2005, 2006–2007, 2009–2010, and 2015–2016 El Niño events), the strong westward-flowing LEIC disappears during the second autumn-winter period (gray shadings in Figures 1h and 1i), corresponding with the presence of strong eastward U_a. Additionally, during the 1997–1998 El Niño event, the modeled disappearance of LEIC from September to December 1998 is consistent with the mooring measurement records at 0°, 138°E (Kawabe et al., 2008, their Figure 3). Given that La Niña events usually have an opposite impact on currents compared to El Niño events, they may cause strong westward U_a in the second autumn-winter period. This is basically established in the observation (2016–2017 and 2017–2018 La Niña events), GL12, and LCS-MR (1995–1996, 1998–1999, 1999–2000, 2000–2001, 2005–2006, 2007–2008, 2008–2009, 2010–2011, 2011–2012, 2016–2017, and 2017–2018 La Niña events). In the following, we will detail how El Niño events influence the LEIC interannual variability by examining the dynamics behind the presence of a strong eastward U_a.

Using the GL12 and LCS-MR outputs, we next construct the composite horizontal distribution of U_a averaged over 600–820 m depths during the preceding and following October–November–December months (denoted as OND(0) and OND(1)) of the 2-year El Niño events. Both models reproduce the interannual

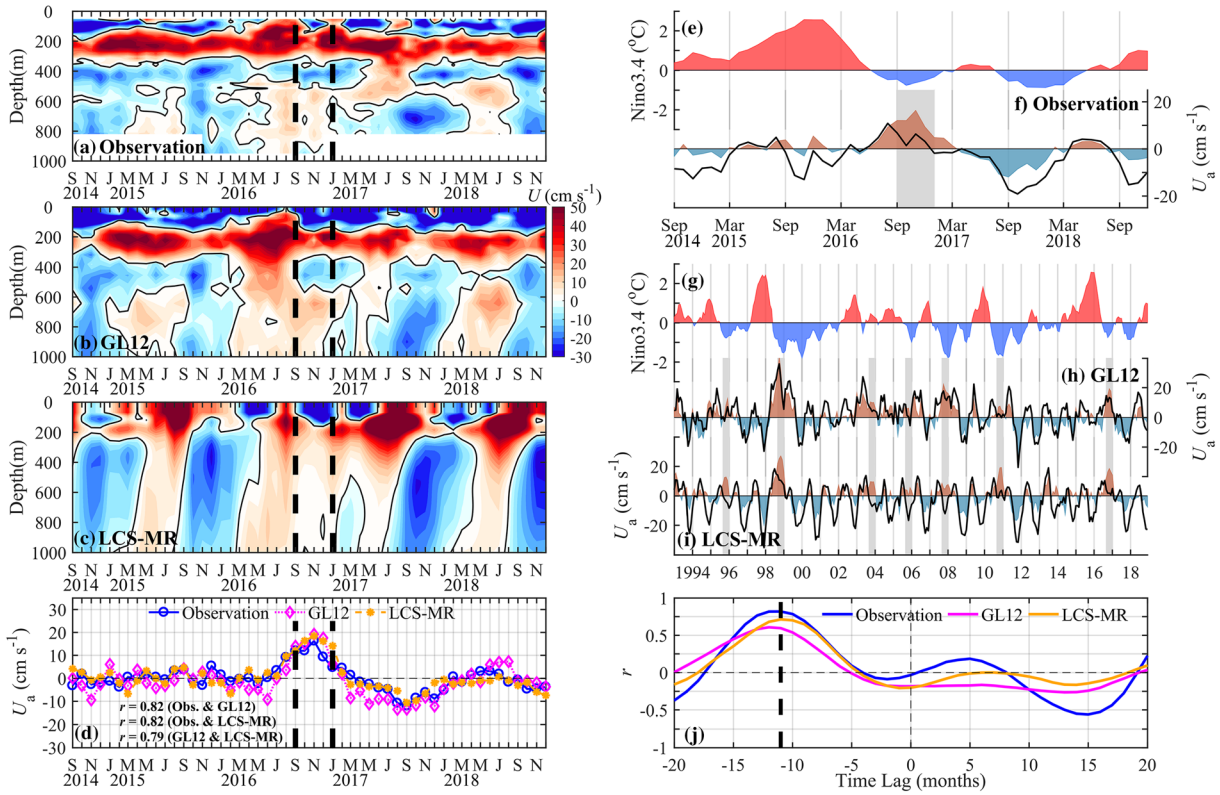

Figure 1. Comparison of time-depth variations of monthly zonal current (U) during September 2014 to December 2018 obtained from (a) the observation, (b) GL12, and (c) LCS-MR at 0°, 142°E. (d) Time series of monthly zonal current anomaly (U_a) averaged over the depths of 600–820 m from the observation (blue), GL12 (magenta), and LCS-MR (orange). The zero-lag correlation coefficients r between them are denoted. Time series of Niño-3.4 index during (e) the observation period and (g) 1993–2018. Temporal variations of U (black line) and U_a (brown and dark green bars) averaged over depths of 600–820 m from (f) the observation, (h) GL12, and (i) LCS-MR. The months corresponding to the disappearance of the strong westward-flowing LEIC are denoted by two dashed lines in panels (a)–(d) and by gray shadings in panels (f), (h), and (i). (j) Lead–lag correlations between Niño-3.4 index and U_a from the observation (blue), GL12 (magenta), and LCS-MR (orange). Negative lags indicate that Niño-3.4 index leads U_a.

changes of equatorial U_a in the western Pacific caused by El Niño events, that is, weak eastward U_a in GL12 or even westward U_a in LCS-MR during OND(0), but strong eastward U_a in both models during OND(1) (Figures 2a–2d).

As the winds are the only external forcing for the LCS-MR, the well-simulated LEIC interannual variability must bear a close relation to the wind changes during El Niño events. On this basis, we plot the longitude-time variations of the composite monthly zonal wind stress anomaly ($\tau^x_{a\_El\ Niño}$) averaged between 5°S and 5°N during all El Niño events from 1993 to 2018 (Figure 3a). The anomaly is obtained by subtracting the monthly climatology to remove the seasonal cycle. The evolution of $\tau^x_{a\_El\ Niño}$ can be divided into three stages: the developing stage from January(0) to August(0) with strengthening westerly $\tau^x_{a\_El\ Niño}$ in the western Pacific, the mature stage from September(0) to April(1) with fully developed westerly $\tau^x_{a\_El\ Niño}$ in the western and central Pacific and weaker easterly $\tau^x_{a\_El\ Niño}$ in the eastern Pacific, and the decaying stage from May(1) to December(1) with gradually strengthening easterly $\tau^x_{a\_El\ Niño}$ in the western Pacific. The $\tau^x_{a\_El\ Niño}$ during the decaying stage indicates the establishment of La Niña-like conditions over the Pacific basin.

To isolate the key stage of the wind evolution for the presence of strong eastward U_a among the three stages, we carry out four numerical experiments using composite monthly wind stresses of the El Niño events over the whole stages (LCS-Case0), only during the developing (LCS-Case1), mature (LCS-Case2), and decaying (LCS-Case3) stages, respectively. LCS-Case0 is used as a control run for the other three experiments. During the residual period in the other three experiments, the monthly climatological wind is exerted. Figure 2e shows that the LCS-Case0 reproduces a strong eastward U_a along the equator during OND(1) in the

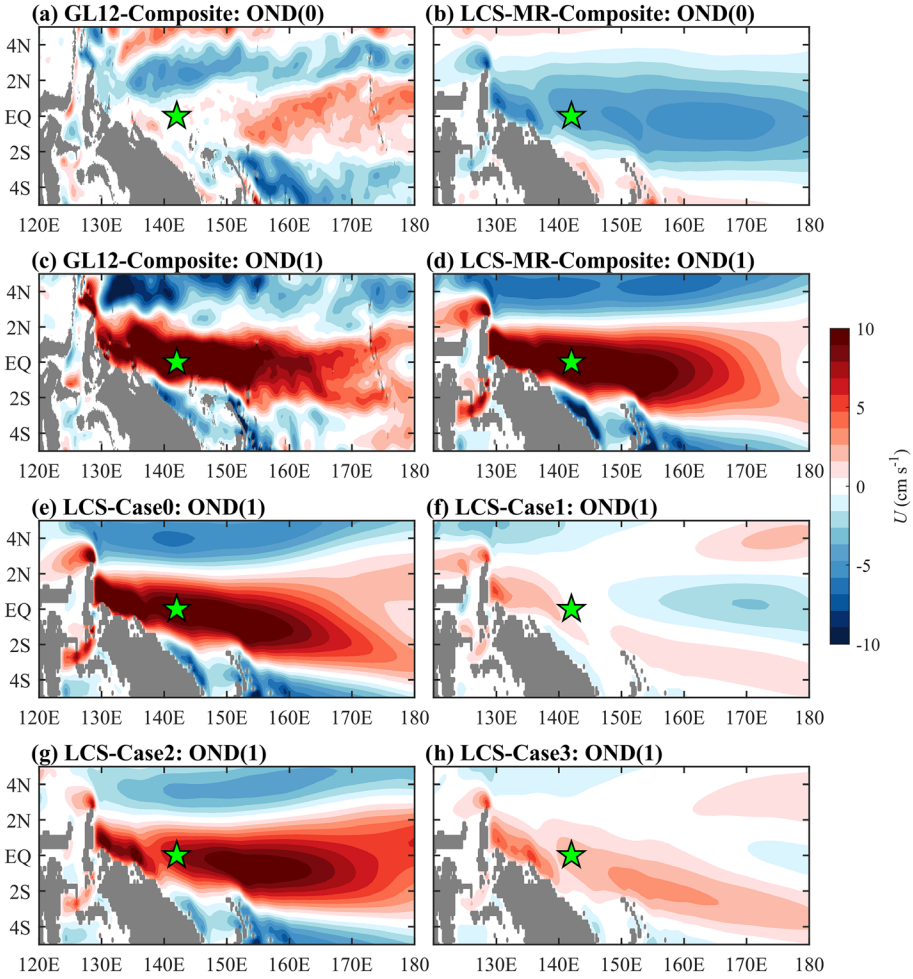

Figure 2. Distributions of composite U_a averaged over 600–820 m depths during (a and b) OND(0) and (c and d) OND(1) of the 2-year El Niño events from (a and c) GL12 and (b and d) LCS-MR. (e–h) Distributions of U_a averaged over 600–820 m depths during OND(1) from the four LCS experiments forced by different wind fields (see the text). The mooring site is denoted by the green pentagram in each panel.

western Pacific. Among the other three experiments, only LCS-Case2 shows a similar result (Figures 2f–2h). This suggests that the wind forcing during the mature stage of El Niño events plays a critical role in the presence of strong eastward U_a during OND(1).

To further explore the dynamics associated with the winds during the mature stage of El Niño events, we examine the composite results from LCS-MR. Figures 3b–3d show the longitude-time plots of SLA along 3°S, the equator, and 3°N. During the mature stage, the westerly wind anomaly in the central Pacific excites equatorial downwelling Kelvin waves (SLA > 0, Figure 3c), which propagate into the eastern Pacific and are reflected back by the eastern boundary as off-equatorial downwelling Rossby waves in both hemispheres at the end of the preceding year (North et al., 2015; Figures 3b and 3d). Meanwhile, the anticyclonic wind stress curl associated with the eastern Pacific easterly wind anomaly can induce off-equatorial westward-propagating downwelling Rossby waves. Under the dominance of the second baroclinic mode (as discussed later), the downwelling Rossby waves, including those from the reflection of Kelvin waves and direct wind forcing, can induce negative pressure anomaly fields (P_a) at 600–820 m along 3°S and 3°N; the values of which are more negative than those at the equator (Figures 3f–3h). The meridional structure of the pressure anomaly fields in the equatorial region is consistent with the meridional eigenfunction of the $l = 1$ Rossby wave (Lukas & Firing, 1985) and can excite an eastward U_a according to the equatorial geostrophy $\left(U_a = -\frac{1}{\bar{\rho}\beta}\frac{\partial^2 P_a}{\partial y^2}\right.$, where $\bar{\rho}$ is background density and β is meridional variation of the Coriolis parameter;

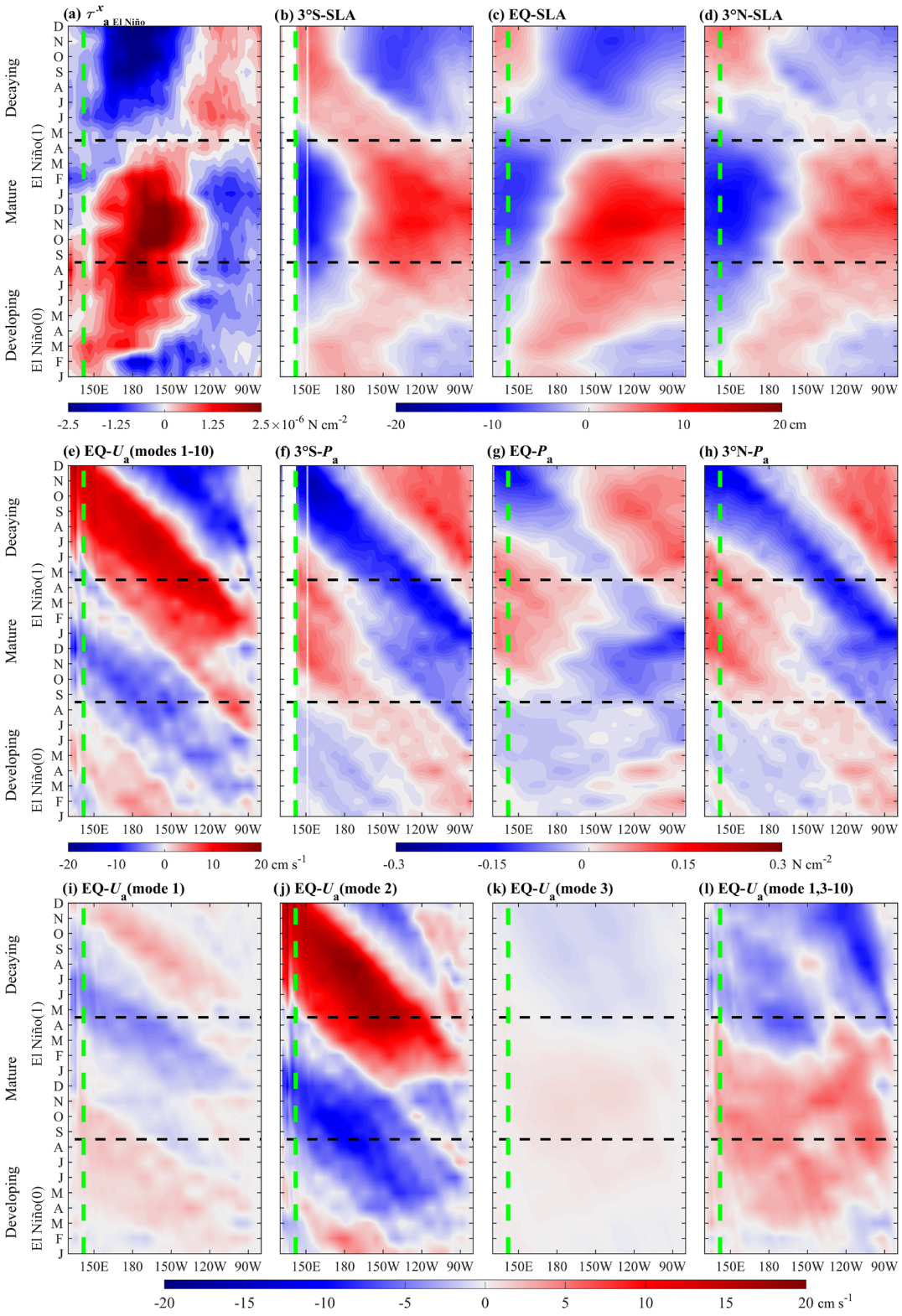

Figure 3. Longitude-time plots of composite (a) zonal wind stress anomaly ($\tau^x_{a\_El\ Niño}$) averaged between 5°S and 5°N and SLA along (b) 3°S, (c) the equator, and (d) 3°N and (e) U_a at the equator from the sum of modes 1–10 and pressure anomaly P_a along (f) 3°S, (g) the equator, and (h) 3°N averaged between 600 and 820 m in LCS-MR. (i–l) Same as panel (e) but from baroclinic modes 1–3 and a sum of modes 1 and 3–10, respectively. The black dashed lines in each panel are used to separate the developing (January(0) to August(0)), mature (September(0) to April(1)), and decaying (May(1) to December(1)) stages based on the $\tau^x_{a\_El\ Niño}$ evolution. The green dashed line in each panel denotes the longitude of the mooring site.

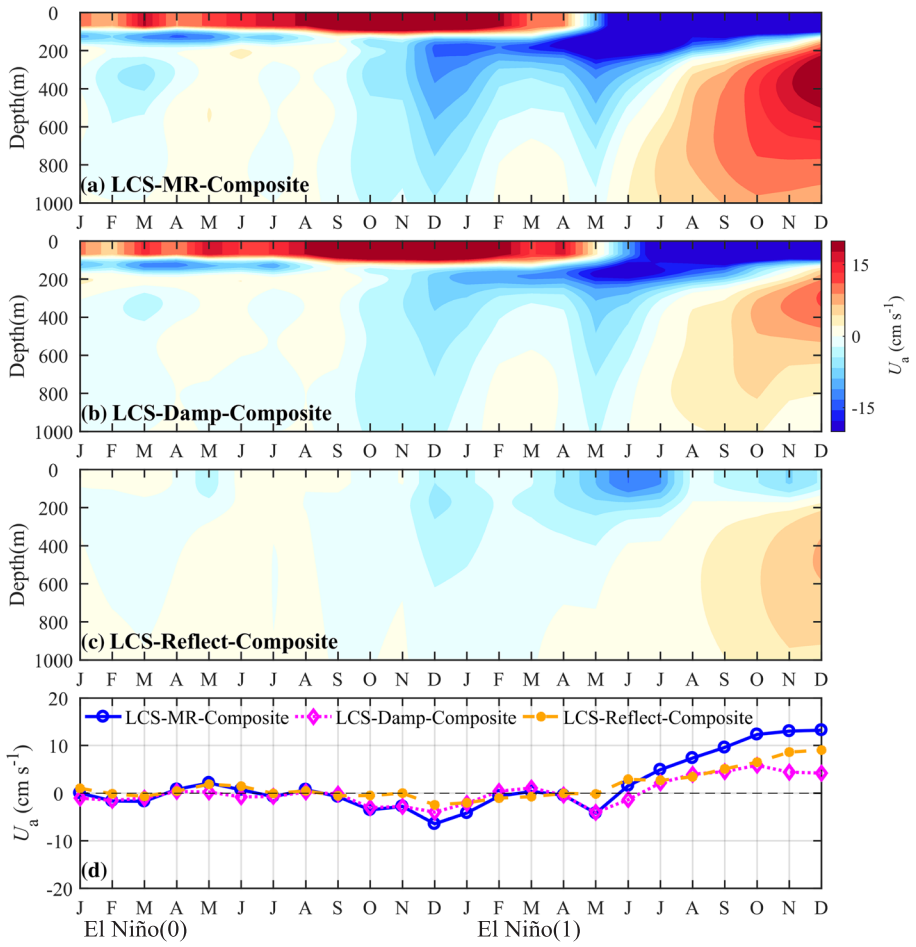

Figure 4. Time-depth variations of monthly U_a at 0°, 142°E obtained from (a) LCS-MR-Composite, (b) LCS-Damp-Composite, and (c) LCS-Reflect-Composite. (d) Time series of U_a averaged between 600–820 m at 0°, 142°E in LCS-MR-Composite (blue), LCS-Damp-Composite (magenta), and LCS-Reflect-Composite (orange).

Chen et al., 2015; Figure 3e). The signal of this eastward U_a propagates westward accompanied by off-equatorial westward-propagating Rossby waves at a phase speed of approximately 51 cm s^{-1} and arrives at the mooring site during September(1) to December(1). Thus, the absence of the strong westward-flowing LEIC in the western Pacific is a delayed (~11 months) ocean response to the strong equatorial wind anomaly over the central-to-eastern Pacific during the mature stage of El Niño events. The above conclusions are also established in GL12 (Figure S2). From the wave dispersion relation ($\omega = -\frac{kc_n}{2l+1}$, where ω is frequency, k is zonal wavenumber, c_n is characteristic wave speed, and l is meridional mode number; Kessler & McCreary, 1993), c_n is estimated to be 153 cm s^{-1} ($c_n = -\frac{\omega(2l+1)}{k} = -c_p(2l+1)$, where c_p is phase speed), which is close to that of the second baroclinic mode ($c_2 = 159$ cm s^{-1}). Furthermore, the longitude-time variation of U_a is largely explained by the second baroclinic mode, which can be clearly inferred from Figures 3e and 3i–3l. These results suggest that the first meridional mode Rossby waves associated with the second baroclinic mode are mainly responsible for the LEIC interannual variability.

The off-equatorial downwelling Rossby waves can be produced from direct easterly wind forcing and reflection of equatorial Kelvin waves in the eastern Pacific. The relative importance of the above two originations deserves to be assessed. To do so, we conduct an experiment using a damper within the region of 7.5°S to 7.5°N and 85°W to 80°W in the eastern Pacific Ocean (LCS-Damp). The experiment is forced by the same winds of LCS-MR. The damper can efficiently absorb the energy of incoming equatorial Kelvin waves;

therefore, no Rossby waves are reflected back into the ocean interior from the eastern boundary. We construct the composite zonal current anomaly at 0°, 142°E during El Niño events from LCS-MR and LCS-Damp, denoted as LCS-MR-Composite and LCS-Damp-Composite, respectively. The difference between them isolates the reflected Rossby wave effects, denoted as LCS-Reflect-Composite. During OND(1) when the strong westward-flowing LEIC disappears, U_a induced by the direct wind forcing and reflected Rossby waves make comparable contributions to the total U_a, inferred from the time-depth plots in Figures 4a–4c. To further quantify this argument, we obtain the time series of U_a averaged between 600 and 820 m from LCS-MR-Composite, LCS-Damp-Composite, and LCS-Reflect-Composite (Figure 4d). The correlations of total U_a with that obtained from LCS-Damp-Composite and LCS-Reflect-Composite are 0.95 and 0.96, respectively, suggesting that their temporal variations are generally in phase. The root-mean-square deviations (RMSDs) of total U_a with that obtained from LCS-Damp-Composite and LCS-Reflect-Composite are 3.36 and 2.70 cm s^{-1}, respectively. The comparable RMSDs further indicate that direct wind forcing and reflected Rossby waves are almost equally crucial for the LEIC interannual variability. This finding roughly applies to the LEIC over longitudes of 135°E to 165°E, and the reflected Rossby waves make more significant contributions to the interannual variability over the longitudes east of 165°E (Figure S3).

For La Niña events, the mature stage wind also plays a decisive role in the interannual variability of LEIC compared to the developing and decaying stages (figure not shown). The zonal wind stress anomaly ($\tau^x_{\text{a\_La Niña}}$) during the mature stage of La Niña generally has an opposite condition compared to El Niño events, that is, fully developed easterly $\tau^x_{\text{a\_La Niña}}$ in the western and central Pacific and weaker westerly $\tau^x_{\text{a\_La Niña}}$ in the eastern Pacific. The off-equatorial westward-propagating upwelling Rossby waves are excited by the cyclonic wind stress curl associated with the eastern Pacific westerly wind anomaly and by the eastern boundary reflection of equatorial upwelling Kelvin waves initially triggered by the easterly wind anomaly in the central Pacific. Under the dominance of the second baroclinic mode, the direct wind forcing and reflected upwelling Rossby waves can equally induce a signal of westward U_a along the equator at the LEIC depths.

4. Summary and Discussion

Based on a 4-year mooring record of zonal currents at 0°, 142°E, the mean westward-flowing LEIC is found to have significant interannual variability. The LCS model and GL12 product faithfully reproduce the observed LEIC interannual variability and thus are used to explore its underlying dynamics. The correlations of the observed LEIC U_a during 2014–2018 and GL12 and LCS modeled U_a during 1993–2018 with the Niño-3.4 index all show significant peak values larger than 0.61 at an approximately 11-month lag. This suggests that the LEIC interannual variability is strongly influenced by the ENSO cycle.

By conducting a series of LCS experiments, we demonstrate that the interannual variability is closely associated with wind changes during the ENSO mature stage (i.e., September(0) to April(1)). For El Niño (La Niña) events, the off-equatorial westward-propagating downwelling (upwelling) $l = 1$ Rossby waves are excited by the anticyclonic (cyclonic) wind stress curl associated with the equatorial easterly (westerly) wind anomaly in the eastern Pacific and by the eastern boundary reflection of equatorial downwelling (upwelling) Kelvin waves initially triggered by the westerly (easterly) wind anomaly in the central Pacific. Under the dominance of the second baroclinic mode, these Rossby waves make the second order meridional derivative of the intermediate-depth pressure anomaly from 3°S to 3°N negative (positive) and thus a signal of eastward (westward) U_a at the equator according to the equatorial geostrophy. This signal of eastward (westward) U_a in the eastern Pacific propagates westward and arrives at the mooring site in ~11 months during September(1) to December(1). Rossby waves from the direct wind forcing and reflection of Kelvin waves make comparable contributions to the interannual variability of LEIC.

Considering that the observation period in this study only covers the 2015–2016 El Niño event, we cannot yet make full conclusions about the interannual viability of EICs. For example, given that the wind field evolution during each El Niño event is different, the discrepancies among the responses of the LEIC to different El Niño events are overlooked in our composite analysis and would be interesting topics for future studies.

The presence of the western boundary and the Papua New Guinea coast makes the western Pacific a narrowed accumulation region for intermediate currents. Figures 3f–3h show that anomalous intermediate

P_a intensifies near the western boundary. This can generate an enhanced magnitude of equatorial U_a (Figure 3e), suggesting the potential effect of the western boundary on LEIC variability in the western Pacific. Furthermore, the LEIC and the intermediate New Guinea Coastal Undercurrent (NGCUC) have an interconnected relationship. Previous studies (Kawabe et al., 2008; Zenk et al., 2005) and GL12 outputs (figure not shown) both reveal that the LEIC and NGCUC reverse seasonally with a nearly opposite phase. The seasonal-to-interannual variability of the LEIC and NGCUC can work together to influence the water-mass distribution along the equator and in the entrance region of the Indonesian Throughflow (ITF), which is the only pathway for the interocean exchange of tropical waters between the Pacific and Indian Oceans (Gordon et al., 2008, 2019; Gordon & Fine, 1996; Sprintall et al., 2014). When the LEIC reverses to an eastward-flowing current, the Antarctic Intermediate Water (AAIW) carried by the NGCUC mainly turns clockwise to spread eastward along the equator. In contrast, when the LEIC flows westward, the AAIW can intrude northward along the western boundary into the entrance region of the ITF (figure not shown). The question is still open, and more observations and numerical simulations are necessary to examine the intermediate circulation system in the western Pacific.

Data Availability Statement

Mooring data analyzed in this paper are available for download at https://zenodo.org/record/3889352. CCMP sea surface wind data are downloaded from http://www.remss.com/measurements/ccmp. The GL12 product is available on the Copernicus Marine Environment Monitoring Service website (https://resources.marine.copernicus.eu/?option=com_csw&view=details&product_id=GLOBAL_REANALYSIS_PHY_001_030). The Niño-3.4 index can be downloaded from https://psl.noaa.gov/gcos_wgsp/Timeseries/Data/nino34.long.anom.data.

Acknowledgments

We thank Prof. Shankar at the CSIR-National Institute of Oceanography and Dr. Abhisek Chatterjee and Dr. Arnab Mukherjee at the Indian National Centre for Ocean Information Services for providing the numerical model code. Suggestions from Prof. Yuanlong Li and Prof. Chuanyu Liu are greatly appreciated. We are sincerely grateful to all the researchers, staff, and the crew of R/V Kexue (Science) for their efforts in conducting the mooring measurements. Comments from two anonymous reviewers help to improve the manuscript substantially. This study is supported by the National Natural Science Foundation of China (grants 91958204 and 41776022), the Strategic Priority Research Program of the Chinese Academy of Sciences (grant XDA22000000), and the Key Research Program of Frontier Sciences, CAS (grant QYZDB-SSW-SYS034). F. Wang thanks the support from the Scientific and Technological Innovation Project by Qingdao National Laboratory for Marine Science and Technology (grant 2016ASKJ12), the National Program on Global Change and Air-Sea Interaction (grant GASI-IPOVAI-01-01), and the National Natural Science Foundation of China (grants 41730534 and 41421005).

References

Ascani, F., Firing, E., McCreary, J. P., Brandt, P., & Greatbatch, R. J. (2015). The deep equatorial ocean circulation in wind-forced numerical solutions. *Journal of Physical Oceanography*, *45*(6), 1709–1734. https://doi.org/10.1175/JPO-D-14-0171.1

Atlas, R., Ardizzone, J., & Hoffman, R. N. (2008). Application of satellite surface wind data to ocean wind analysis. Remote Sensing System Engineering, Proceedings SPIE, Vol. *7087*, 70870B. https://doi.org/10.1117/12.795371

Brandt, P., Funk, A., Hormann, V., Dengler, M., Greatbatch, R. J., & Toole, J. M. (2011). Interannual atmospheric variability forced by the deep equatorial Atlantic Ocean. *Nature*, *473*(7348), 497–500. https://doi.org/10.1038/nature10013

Chatterjee, A., Shankar, D., McCreary, J. P. Jr., & Vinayachandran, P. N. (2013). Yanai waves in the western equatorial Indian Ocean. *Journal of Geophysical Research: Oceans*, *118*, 1556–1570. https://doi.org/10.1002/jgrc.20121

Chen, G., Han, W., Li, Y., Wang, D., & McPhaden, M. J. (2015). Seasonal-to-interannual time-scale dynamics of the Equatorial Undercurrent in the Indian Ocean. *Journal of Physical Oceanography*, *45*(6), 1532–1553. https://doi.org/10.1175/JPO-D-14-0225.1

Cravatte, S., Kestenare, E., Marin, F., Dutrieux, P., & Firing, E. (2017). Subthermocline and intermediate zonal currents in the tropical Pacific Ocean: Paths and vertical structure. *Journal of Physical Oceanography*, *47*(9), 2305–2324. https://doi.org/10.1175/JPO-D-17-0043.1

Czeschel, R., Stramma, L., Schwarzkopf, F. U., Giese, B. S., Funk, A., & Karstensen, J. (2011). Middepth circulation of the eastern tropical South Pacific and its link to the oxygen minimum zone. *Journal of Geophysical Research*, *116*, C01015. https://doi.org/10.1029/2010JC006565

Firing, E. (1987). Deep zonal currents in the central equatorial Pacific. *Journal of Marine Research*, *45*(4), 791–812. https://doi.org/10.1357/002224087788327163

Firing, E., Wijffels, S. E., & Hacker, P. (1998). Equatorial subthermocline currents across the Pacific. *Journal of Geophysical Research*, *103*(C10), 21,413–21,423. https://doi.org/10.1029/98JC01944

Gordon, A. L., & Fine, R. A. (1996). Pathways of water between the Pacific and Indian oceans in the Indonesian seas. *Nature*, *379*(6561), 146–149. https://doi.org/10.1038/379146a0

Gordon, A. L., Napitu, A., Huber, B. A., Gruenburg, L. K., Pujiana, K., Agustiadi, T., et al. (2019). Makassar Strait throughflow seasonal and interannual variability: An overview. *Journal of Geophysical Research: Oceans*, *124*, 3737–3754. https://doi.org/10.1029/2018JC014574

Gordon, A. L., Susanto, R. D., Ffield, A., Huber, B. A., Pranowo, W., & Wirasantosa, S. (2008). Makassar Strait throughflow, 2004 to 2006. *Geophysical Research Letters*, *35*, L24605. https://doi.org/10.1029/2008GL036372

Gouriou, Y., Delcroix, T., & Eldin, G. (2006). Upper and intermediate circulation in the western equatorial Pacific Ocean in October 1999 and April 2000. *Geophysical Research Letters*, *33*, L10603. https://doi.org/10.1029/2006GL025941

Hu, D., Wu, L., Cai, W., Gupta, A. S., Ganachaud, A., Qiu, B., et al. (2015). Pacific western boundary currents and their roles in climate. *Nature*, *522*(7556), 299–308. https://doi.org/10.1038/nature14504

Huang, K., Han, W., Wang, D., Wang, W., Xie, Q., Chen, J., & Chen, G. (2018). Features of the Equatorial Intermediate Current associated with basin resonance in the Indian Ocean. *Journal of Physical Oceanography*, *48*(6), 1333–1347. https://doi.org/10.1175/JPO-D-17-0238.1

Izumo, T. (2005). The equatorial undercurrent, meridional overturning circulation, and their roles in mass and heat exchanges during El Niño events in the tropical Pacific Ocean. *Ocean Dynamics*, *55*(2), 110–123. https://doi.org/10.1007/s10236-005-0115-1

Johnson, G. C., & Birnbaum, A. N. (2016). Equatorial Pacific Thermostad response to El Niño. *Journal of Geophysical Research: Oceans*, *121*, 8368–8378. https://doi.org/10.1002/2016JC012304

Johnson, G. C., McPhaden, M. J., Rowe, G. D., & McTaggart, K. E. (2000). Upper equatorial Pacific Ocean current and salinity variability during the 1996-1998 El Niño–La Niña cycle. *Journal of Geophysical Research*, *105*(C1), 1037–1053. https://doi.org/10.1029/1999JC900280

Kawabe, M., Kashino, Y., & Kuroda, Y. (2008). Variability and linkages of New Guinea coastal undercurrent and lower equatorial intermediate current. *Journal of Physical Oceanography*, *38*(8), 1780–1793. https://doi.org/10.1175/2008JPO3916.1

Kessler, W. S., & McCreary, J. P. (1993). The annual wind-driven Rossby wave in the subthermocline equatorial Pacific. *Journal of Physical Oceanography*, *23*(6), 1192–1207. https://doi.org/10.1175/1520-0485(1993)023<1192:TAWDRW>2.0.CO;2

Lellouche, J.-M., Greiner, E., le Galloudec, O., Garric, G., Regnier, C., Drevillon, M., et al. (2018). Recent updates to the Copernicus Marine Service global ocean monitoring and forecasting real-time 1/12° high-resolution system. *Ocean Science*, *14*(5), 1093–1126. https://doi.org/10.5194/os-14-1093-2018

Lukas, R., & Firing, E. (1985). The annual Rossby wave in the central equatorial Pacific Ocean. *Journal of Physical Oceanography*, *15*(1), 55–67. https://doi.org/10.1175/1520-0485(1985)015<0055:TARWIT>2.0.CO;2

Lyu, Y., Li, Y., Tang, X., Wang, F., & Wang, J. (2018). Contrasting intraseasonal variations of the equatorial Pacific Ocean between the 1997-1998 and 2015-2016 El Niño events. *Geophysical Research Letters*, *45*, 9748–9756. https://doi.org/10.1029/2018GL078915

Ma, Q., Wang, F., Wang, J., & Lyu, Y. (2019). Intensified deep ocean variability induced by topographic Rossby waves at the Pacific Yap-Mariana Junction. *Journal of Geophysical Research: Oceans*, *124*, 8360–8374. https://doi.org/10.1029/2019JC015490

Margolskee, A., Frenzel, H., Emerson, S., & Deutsch, C. (2019). Ventilation pathways for the North Pacific oxygen deficient zone. *Global Biogeochemical Cycles*, *33*, 875–890. https://doi.org/10.1029/2018GB006149

Marin, F., Kestenare, E., Delcroix, T., Durand, F., Cravatte, S., Eldin, G., & Bourdallé-Badie, R. (2010). Annual reversal of the Equatorial Intermediate Current in the Pacific: Observations and model diagnostics. *Journal of Physical Oceanography*, *40*(5), 915–933. https://doi.org/10.1175/2009JPO4318.1

Ménesguen, C., Delpech, A., Marin, F., Cravatte, S., Schopp, R., & Morel, Y. (2019). Observations and mechanisms for the formation of deep equatorial and tropical circulation. *Earth and Space Science*, *6*, 370–386. https://doi.org/10.1029/2018EA000438

North, G. R., Pyle, J. A., & Zhang, F. (2015). *Encyclopedia of atmospheric sciences* (2nd ed. pp. 347–352). Amsterdam: Elsevier/Academic Press. https://doi.org/10.1016/B978-0-12-382225-3.00191-2

Shankar, D., McCreary, J. P., Han, W., & Shetye, S. R. (1996). Dynamics of the East India Coastal Current: 1. Analytic solutions forced by interior Ekman pumping and local alongshore winds. *Journal of Geophysical Research*, *101*(C6), 13,975–13,991. https://doi.org/10.1029/96JC00559

Shinoda, T., Hurlburt, H. E., & Metzger, E. J. (2011). Anomalous tropical ocean circulation associated with La Niña Modoki. *Journal of Geophysical Research*, *116*, C12001. https://doi.org/10.1029/2011JC007304

Song, L., Li, Y., Wang, J., Wang, F., Hu, S., Liu, C., et al. (2018). Tropical meridional overturning circulation observed by subsurface moorings in the Western Pacific. *Scientific Reports*, *8*(1), 7632. https://doi.org/10.1038/s41598-018-26047-7

Sprintall, J., Gordon, A. L., Koch-Larrouy, A., Lee, T., Potemra, J. T., Pujiana, K., & Wijffels, S. E. (2014). The Indonesian seas and their role in the coupled ocean–climate system. *Nature Geoscience*, *7*(7), 487–492. https://doi.org/10.1038/ngeo2188

Stramma, L., Johnson, G. C., Firing, E., & Schmidtko, S. (2010). Eastern Pacific oxygen minimum zones: Supply paths and multidecadal changes. *Journal of Geophysical Research*, *115*, C09011. https://doi.org/10.1029/2009JC005976

Wang, F., Li, Y., & Wang, J. (2016). Intraseasonal variability of the surface zonal currents in the western tropical Pacific Ocean: Characteristics and mechanisms. *Journal of Physical Oceanography*, *46*, 3639–3660. https://doi.org/10.1175/JPO-D-16-0033.1

Wang, F., Wang, J., Guan, C., Ma, Q., & Zhang, D. (2016). Mooring observations of equatorial currents in the upper 1000 m of the western Pacific Ocean during 2014. *Journal of Geophysical Research: Oceans*, *121*, 3730–3740. https://doi.org/10.1002/2015JC011510

Yu, X., & McPhaden, M. J. (1999). Seasonal variability in the equatorial Pacific. *Journal of Physical Oceanography*, *29*(5), 925–947. https://doi.org/10.1175/1520-0485(1999)029<0925:SVITEP>2.0.CO;2

Zanowski, H., Johnson, G. C., & Lyman, J. M. (2019). Equatorial pacific 1,000-dbar velocity and isotherm displacements from Argo data: Beyond the mean and seasonal cycle. *Journal of Geophysical Research: Oceans*, *124*, 7873–7882. https://doi.org/10.1029/2019JC015032

Zenk, W., Siedler, G., Ishida, A., Holfort, J., Kashino, Y., Kuroda, Y., et al. (2005). Pathways and variability of the Antarctic Intermediate Water in the western equatorial Pacific Ocean. *Progress in Oceanography*, *67*(1–2), 245–281. https://doi.org/10.1016/j.pocean.2005.05.003

Zhao, J., Li, Y., & Wang, F. (2013). Dynamical responses of the west Pacific North Equatorial Countercurrent (NECC) system to El Niño events. *Journal of Geophysical Research: Oceans*, *118*, 2828–2844. https://doi.org/10.1002/jgrc.20196